



## FIELD REPORT

# Remote sensing and identification of volcanic plumes using fixed-wing UAVs over Volcán de Fuego, Guatemala

Ben Schellenberg<sup>1</sup>  | Tom Richardson<sup>1</sup> | Matt Watson<sup>2</sup> | Colin Greatwood<sup>1</sup> | Robert Clarke<sup>1</sup> | Rick Thomas<sup>3</sup> | Kieran Wood<sup>1</sup>  | Jim Freer<sup>4</sup> | Helen Thomas<sup>2</sup> | Emma Liu<sup>5</sup> | Francis Salama<sup>6</sup> | Gustavo Chigna<sup>7</sup>

<sup>1</sup>Department of Aerospace Engineering, University of Bristol, Bristol, UK

<sup>2</sup>School of Earth Sciences, University of Bristol, Bristol, UK

<sup>3</sup>School of Geography, Earth and Environmental Sciences, University of Birmingham, Birmingham, UK

<sup>4</sup>School of Geographical Sciences, University of Bristol, Bristol, UK

<sup>5</sup>Department of Earth Sciences, University of Cambridge, Cambridge, UK

<sup>6</sup>BlueBear Systems, Bedford, UK

<sup>7</sup>INSIVUMEH, Edificio Central, Guatemala City, Guatemala

## Correspondence

Ben Schellenberg, Department of Aerospace Engineering, University of Bristol, Bristol BS8 1TR, UK.

Email: ben.schellenberg@bristol.ac.uk

## Funding information

Engineering and Physical Sciences Research Council, Grant/Award Number: EP/R009953/1

## Abstract

This paper describes a series of proof-of-concept Beyond Visual Line Of Sight unmanned aerial vehicle flights which reached a range of up to 9 km and an altitude of 4,410 m Above Mean Sea Level over Volcán de Fuego in Guatemala, interacting with the volcanic plume on multiple occasions across a range of different conditions. Volcán de Fuego is an active volcano which emits gas and ash regularly, causing disruption to airlines operating from the international airport 50 km away and impacting the lives of the local population. Collection of data from within the plume develops scientists' understanding of the composition of the volcano's output and is of use to scientists, aviation, and hazard management groups alike. This paper presents preliminary results of multiple plume interceptions with multiple aircraft, carrying a variety of sensors. A plume-detection metric is introduced, which uses a combination of flight data and atmospheric sensor data to identify flight through a volcanic plume. Future work will develop the automation of plume tracking such that reliable scientific data sets can be gathered in a robust manner.

## KEYWORDS

aerial robotics, environmental monitoring

## 1 | INTRODUCTION

### 1.1 | Motivation

Volcanoes are significant point source emitters of ash, gas, and aerosols to the atmosphere. Volcanic ash, particularly fine ash measuring  $<63 \mu\text{m}$ , has been proven to have a profound effect on the operation of both civil and military aviation (Clarkson, Majewicz, & Mack, 2016). Airspace used by aviation is managed operationally using two primary tools: advection-diffusion dispersion models (Stohl et al., 2011), driven by volcanic and meteorological source

terms, and satellite remote sensing (H. E. Thomas & Watson, 2010; Watson et al., 2004). The first offers a forecast, which is vital for flight planners, although forward projection in time increases uncertainty. The latter, whilst also being uncertain, provides snapshots that may be used to validate predictions at a known time but with some notable latency. Both techniques require some information a priori, particularly of the Particle Size Distribution (PSD) and shape of volcanic ash (Mishchenko, 1993; Prata, Volcanic, & Clouds, 1989). Atmospheric conditions (both cloud and thermal effects) can make satellite retrievals challenging, and when combined with significant uncertainty around PSD and shape this reduces the

This is an open access article under the terms of the Creative Commons Attribution License, which permits use, distribution and reproduction in any medium, provided the original work is properly cited.

© 2019 The Authors. *Journal of Field Robotics* Published by Wiley Periodicals, Inc.

accuracy of satellite retrievals and reliability of dispersion model predictions (Western, Watson, & Francis, 2015). Representative ash samples are therefore critical for the effective use of both airspace and industry management tools, to respond to volcanic events accordingly. Additionally, the knowledge gained by analysing such samples can also help mitigate the effects of large eruptions on the local population by better informing local decision makers.

## 1.2 | Volcán de Fuego

Volcán de Fuego (henceforth referred to as Fuego) is an active volcano in Guatemala with a summit altitude of approximately 3,800 m Above Mean Sea Level (AMSL). Short-term small explosions occur multiple times every hour, with larger, more sustained, eruptions every 3–5 weeks. Occasional major eruptions (e.g., June 2018, September 2012, and October 1974) cause large-scale changes to the area's topography and have a significant impact on the local population. Over 1M people live within a 30 km radius of the volcano (Smithsonian Institute, 2002), and the country's international airport is <50 km away, so the volcano poses a large risk to the Guatemalan population, aviation industry, and economy. Whereas other active volcano craters are relatively accessible for scientists, the large volcanic projectiles that are emitted on ballistic trajectories make Fuego a particularly hard volcano from which to collect samples. Ground-based collection of ash that has fallen out of the plume is common and straightforward, however these samples cannot have a PSD representative of the in-plume PSD. Airborne ash collection from within the plume would have a more representative PSD and poses an interesting engineering problem because novel methods must be used.

Figure 1 is a typical view of Fuego from the operations area, and shows the visible part of the plume from two separate eruptions. In conditions, such as these, it is easy to confirm flight through the plume using the visual cameras on-board the unmanned aerial vehicles (UAVs). The weather around Fuego can be unpredictable, and cloud often arrives between the ground and summit altitude around the middle of the day. Even in these conditions the plume is

still visible on camera as it shows up as darker than the normal clouds.

## 1.3 | UAVs for volcanic and atmospheric research

UAVs enable a wide range of operations that would otherwise not be possible due to restrictions on human safety, physical limitations, and do so at a lower cost than most alternative means of gathering data. Everaerts (2008), Wegener (2004), and Klemas (2015) present early papers on the potential use of UAVs for scientific missions, with Everaerts highlighting the usefulness of UAVs for scientific remote sensing and mapping due to the low cost and ease of access to platforms. Klemas compares UAVs for remote sensing over coastal areas with the manned aircraft that were previously used at great expense. UAVs give excellent access to extreme environments, as demonstrated by Di Stefano who used a multicopter to monitor and gather data over the Lusi mud crater in Indonesia (Di Stefano et al., 2017).

Ramanathan et al. (2007) pioneered the use of lightweight fixed-wing UAVs to investigate atmospheric phenomena, equipping three large fixed-wing aircraft with aerosol, soot, and solar radiation instrumentation to measure the heating effect of brown carbon layers between 0.5 and 3 km above the Indian Ocean. They were flown in stacked formation for simultaneous data collection from different altitudes. The additional development of a turbulent flux measurement system for UAVs by R. M. Thomas et al. (2012) enabled further investigations above the Indian Ocean, including the discovery that solar absorption by black carbon particles suppresses boundary layer turbulence (Wilcox et al., 2016). As Thomas notes in the 2012 paper, instruments for taking representative measurements of atmospheric phenomena often need to be out of the boundary layer of the aircraft. These instruments can be a significant component of the overall takeoff mass, leading to challenges with balance and flight control when mounted as required.

Villa, Gonzalez, Miljjevic, Ristovski, and Morawska (2016) review the use of UAVs for air quality studies, assessing their suitability and challenges in their implementation. Although a fundamentally

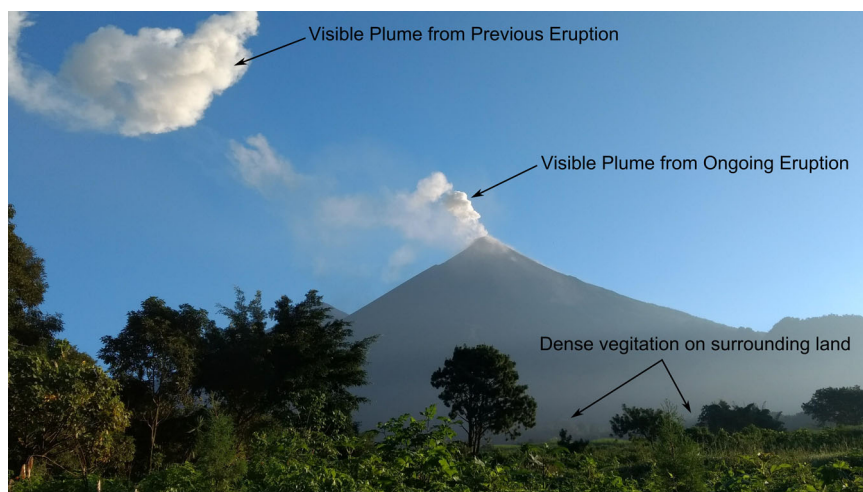


**FIGURE 1** A typical view of Fuego from near the operations point. Note the visible plumes of two small eruptions, and the thick brush in the foreground [Color figure can be viewed at [wileyonlinelibrary.com](http://wileyonlinelibrary.com)]

desirable method of collecting air data, their paper highlights a few key challenges, including a necessity for sensors that are both small and suitably accurate, and overcoming policies/regulations, such as import systems and airspace rules. These factors translate into most other applications of UAVs. Schuyler and Guzman (2017) review the various UAV options available for sampling tropospheric gases, and conclude that fixed-wing aircraft with a wingspan of under 3 m and a payload of <5 kg provide the best compromise between cost and convenience of sensor deployment. Of note here is the value associated with the hours of preparation and testing in research and development of an unmanned system, a factor which is often ignored in the planned use of UAVs for ground-breaking research.

Greatwood et al. (2016, 2017) used multirotor UAVs to collect high-altitude nonvolcanic scientific data, sampling the atmosphere above Ascension Island at approximately 3,000 m AMSL. Large (25 kg) fixed-wing UAVs have been used by Altstädter et al. (2015) to observe ultrafine particle distributions within the atmospheric boundary layer, however these flights only flew to a maximum altitude of 1,080 m AMSL.

UAVs offer outstanding new sampling opportunities for volcanic emissions (Ogiso et al., 2016). The Handbook of UAVs discusses the application of UAVs to volcanic monitoring and sampling, giving some examples of early projects and noting that their results are still preliminary due to the harshness of the environment (Longo, Melita, Muscato, & Giudice, 2014). Gas and ash sensors have been miniaturised enough to be flown on UAVs and are able to provide real-time information and, in principle, capture and retrieve samples. UAVs allow direct and remote measurements much closer to volcanic vents than previously possible at volcanoes, such as Fuego, leading to better characterisation of the plume. Autopilot hardware and navigation algorithms improve repeatability, which should serve to better validate satellite and ground-based remote observations. Depending on the sensor and aim of collection, different UAVs can be used; for example, sampling a single location near a vent would be suited best to a multirotor UAV, but longer flight times and higher distances can be achieved by fixed-wing UAVs so they are better suited to sampling at varying distal ranges from the crater.

The first reported use of UAVs over volcanoes for scientific purposes was by McGonigle et al. (2008) in 2007, who used a helicopter UAV with a payload capacity of 3 kg at La Fossa crater in Italy. Amici et al. (2013) report the development of multirotor and fixed-wing UAV flights over Stromboli volcano in Italy, however they focus on the successes of a hexacopter with a thermal camera on-board. Jordan (2015) presents a short summary of UAVs in geology, focusing on small multirotors, such as DJI Phantoms (DJI, Shenzhen, China) and the challenges surrounding their use in scientific fieldwork. Whereas Fuego's activity involves large ballistics, active volcanoes, such as Turrialba and Masaya in Central America, are safer to be close to, hence TakeOff/Land Points (TOLPs) can be found relatively close to the craters (Stix et al., 2018). As Stix et al. show, with minimal altitude gain and short ranges required, multirotors are ideal platforms for sensor placement in static locations for gas measurements. These works consider volcanoes which are relatively

accessible and note flight times between 12 and 15 min. Some areas of interest, such as Fuego, are dangerous to approach, meaning that flight times must be longer and cruise speeds higher to reach them from a safe distance. Fixed-wing UAVs are a natural solution to this issue, as demonstrated by Pieri et al. (2013), who flew fixed-wing UAVs over Turrialba, while also flying 'tethersonde' meteorological balloons for data verification. Primarily sensing gases, these experiments validated the use of UAVs in scientific data collection over volcanoes, specifically delta-wing style fixed-wing aircraft.

#### 1.4 | UAVs at Volcán de Fuego

With an estimated summit altitude of 3,760 m AMSL, a UAV that flies over Fuego must be equipped with the appropriate components to allow for safe, reliable, and useful operations. Paredes, Saito, Abarca, and Cuellar (2017) investigate the effects of high altitude on UAV performance, validating theories generated from background aeronautical knowledge with fixed-wing flights at over 5,500 m AMSL. Parades concludes that energy requirements increase with target altitude, which in turn decreases flight time given a fixed capacity of energy on-board.

INSIVUMEH is the Guatemalan Institute of Seismology, Volcanology, Meteorology, and Hydrology, and work to monitor sites, such as Fuego, to better understand the underlying activity and recommend evacuations when and where necessary. Before these campaigns, the summit of Fuego had last been closely observed in 2012 by manned aircraft, according to local INSIVUMEH observers. Although macroscale behaviour of the volcano can already be monitored with seismometers, cameras, spectrometers, and satellites, close-range behaviour and topography of the summit changes regularly and remains largely unknown, as does the make-up of the volcanic emissions. As the literature shows, UAVs provide unprecedented access to hazardous, often inaccessible, zones around volcanoes. To increase the accuracy of aviation management tools, which would allow for safer operations out of the nearby international airport, a better understanding of the PSD within the plume is desirable.

Although multirotors have their place in remote sensing, particularly where static data acquisition is advantageous, operating them over Fuego's summit involves several hours travel each day just to get to the TOLP, on a road that is impassable for much of the year. The greater range of fixed-wing vehicles relative to multirotors often allows the base of operations to be located at more favourable locations with access to shelter and power. Minimising operators' travel time and logistical issues should enable UAV-based measurements to be more effectively integrated into regular operational monitoring capabilities. The availability of various TOLPs in the area means that, given a sufficient weather window, year-round flights should be possible even if the primary TOLP is inaccessible.

Challenges associated with operating in this region include the large distances and altitude gains required to reach above summit altitude, and overcoming the low air density that is inherent to such 'hot and high' locations. The work presented here made use of a

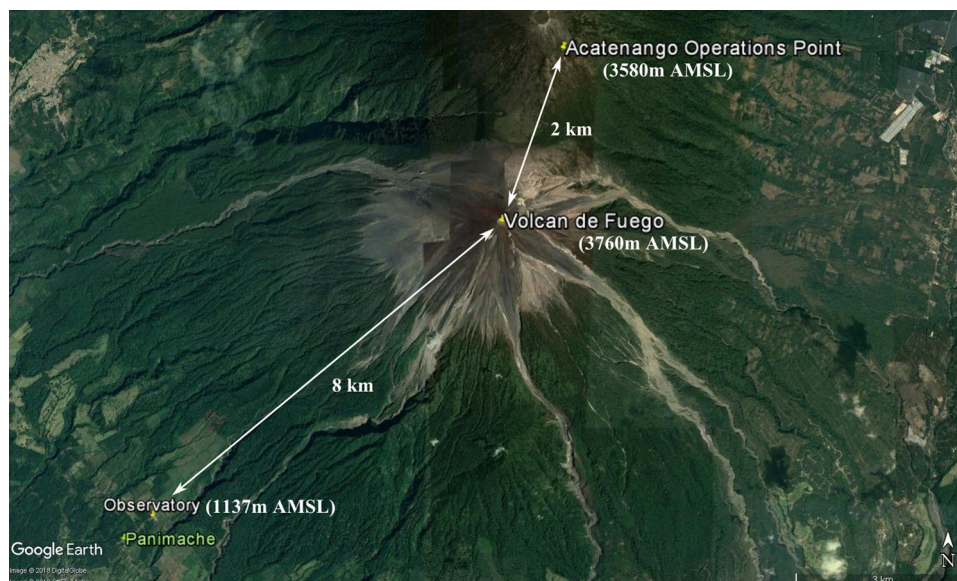


**FIGURE 2** A top-down view of the area and two main TOLPs surrounding Volcán de Fuego (Google Earth, 2018). TOLP, TakeOff/Land Point [Color figure can be viewed at [wileyonlinelibrary.com](http://wileyonlinelibrary.com)]

single TOLP for fixed-wing aircraft; the INSIVUMEH Observatory located just north of Panimache, approximately 8 km South-West of Fuego's summit (Figure 2). This is where the Ground Control Station (GCS) was located for the UAV missions described in this paper.

### 1.5 | Automated plume detection

Fixed-wing UAVs have not been used to collect volcanic data from Fuego before. A typical mission aim is to operate for as long as possible in the section of interest in the plume, for example, to collect ash from the plume between 0.3 and 3 km from the summit, from crater altitude to approximately 500 m above.

Typical UAV flight plans require the mission path to be defined by a number of waypoints before takeoff. Communications difficulties can arise when attempting to change the mission midflight, especially at long range. Should a partial mission be received by the aircraft, unexpected behaviour may follow, in the worst case leading to loss of aircraft. This mission planning method means that, for the best chance of intercepting the plume, the plume bearing and altitude must be determined preflight. This is a challenge due to the parallax error introduced by single-point ground measurements and is subject to good weather conditions. A system of observers and instruments situated at various points around the volcano could be used, however the challenging logistics, human error, and weather conditions make this unattractive. Provided there is still sufficient signal strength for telemetry, control, and video, it is possible for the pilot to take control of the aircraft in a Fly-By-Wire (FBW) mode to navigate towards the plume visually. Although likely to succeed on a case-by-case basis, from an analysis perspective this is an uncontrolled method and inconsistent between flights. It would be preferable to have an automated plume-detection system to reliably intercept the plume. The aircraft should autonomously takeoff, find the plume,

collect the appropriate data, and then return to the GCS to land. The removal of human input from the system poses an interesting problem and one that, if solved, would reduce the risk of mission failure, increase repeatability, and allow nonexperts to make use of the system.

Automated takeoffs and landings have been presented on numerous occasions and are regularly used by UAV operators. The detection of plumes has been investigated by Montes, Letheren, Villa, and Gonzalez (2014) and Letheren and Montes (2016), for finding the source of forest fire plumes using multirotor aircraft. Finding the plume involves the aircraft processing real-time data to establish whether contact with the plume has been made, preferably using sensors that do not conflict with scientific instruments on-board so that independence may be maintained. Letheren's system detected the (fire) plume by sensing CO<sub>2</sub>, and the algorithm they implemented targeted finding the source of the plume. At Fuego, the aim would be to sample specific points in the plume rather than to find its source. The algorithm(s) used on a fixed-wing aircraft for plume detection and tracking must differ from those used on multirotors because a significant forward speed must always be maintained with fixed-wing aircraft.

### 1.6 | Research aims

The purpose of this paper is to establish a preliminary data set for the development of a system that uses UAVs to autonomously sense and quantify aspects of volcanic plumes, and to develop a metric that could be used for reliable plume detection. Clear identification of plumes would allow tracking methods, such as those used by Letheren and Montes (2016), to be implemented, enabling reliable and consistent interaction with the plume.

The hypothesis is that it is possible to detect UAV/Volcanic Plume interaction over Volcán de Fuego using a combination of temperature, ambient relative humidity, and vertical acceleration. A combination of

these data would make up a suitable metric for determining whether or not a UAV is in a plume. Specific behaviours of the UAV can then be implemented to maintain contact with the plume and collect scientific data in a controlled and repeatable manner.

The development of a system with minimal mass and power requirements maximises the usable payload of the aircraft for scientific sensors. Temperature and humidity sensors are typically small, and the on-board autopilot has integrated accelerometers. Additional sensing methods are available, however if it is preferable to sense and identify the plume without the excess weight if possible.

To test the hypothesis, UAVs must be flown through the plume of Fuego multiple times with a variety of sensing methods on-board, so that plume-interception data can be collected by the appropriate sensors and verified by secondary methods. Should the hypothesis be found true, the automation of plume detection is a natural next step.

## 2 | METHODOLOGY AND SYSTEMS

### 2.1 | Operating environment

The INSIVUMEH Observatory is at 1,137 m AMSL which, combined with the tropical climate, leads to challenging 'hot and high' conditions. Pressure decreases with altitude and air temperature, which in turn reduces the air density. For a given amount of lift a reduction in density must be compensated for by another term, the most effective being velocity due to the exponent. Table 1 compares the International Standard Atmosphere (ISA) standard day air-data values to those found at 4,000 m AMSL, approximately 300 m above Fuego's summit. All other parameters remaining constant, the lift generated at maximum altitude was 63.6% of standard day lift, and 77% of 'takeoff lift' at the GCS. Assuming the aircraft remains straight and level this requires a significant increase in both stall and cruise speeds.

There were a number of challenges involved with operating from the Observatory, mostly related to the remote nature of the site. One of the main issues there was takeoff and landing in these 'hot and high' conditions, the flight points at which airspeed is arguably most critical. Much of the land around Fuego is taken up by plantations, with remaining space usually unfarmable; undulating and covered in dense brush. A catapult launch was chosen to ensure the vehicle reliably reached the higher takeoff velocity required.

**TABLE 1** Air and lift data values at the Observatory GCS and approximately 300 m above the summit of Fuego, with ISA standard day values for comparison

Parameter	ISA standard day	Observatory	Target altitude
Altitude (m AMSL)	0	1,137	4,000
Pressure (kPa)	101.3	89.3	63.4
Temperature (°C)	15	34	10
Density (kg/m <sup>3</sup> )	1.225	1.013	0.780
Equivalent lift (%)	100	82.6	63.6

Abbreviations: AMSL, Above Mean Sea Level; GCS, Ground Control Station; ISA, International Standard Atmosphere.

Operating Beyond Visual Line Of Sight (BVLOS) in any country requires liaison with the National Aviation Authority (NAA) to ensure compliance with local regulations. The team worked closely with the Guatemalan NAA, DGAC, to issue NOTAMs (NOTICE To AirMen) for the periods and areas of operation.

### 2.2 | Aircraft and system selection

The work presented here spans three campaigns: in February 2017, November 2017, and October 2018. Two flying-wing aircraft were used: the RiteWing Zephyr II (RiteWing, Apache Junction, AZ) (Figure 3b) as an initial proof-of-concept aircraft for the first campaign and the Skywalker X8 (Skywalker, Guangdong, China) (Figures 3b and 4) for the second and third campaigns. Details of the two vehicles are given in Table 2, including the avionics. Both aircraft were available as hobbyist kits and were assembled in a bespoke configuration for this project. The lack of significant vertical fins mean flying-wings must typically cruise at a relatively high airspeed for a given aircraft size, to avoid dutch roll instabilities and tip stalls. The Skywalker was chosen because the airframe offers a large payload bay and their high cruise speed suited the planned mission distances.

The Zephyr II and Skywalkers were fitted with autopilot systems running ArduPlane, an open-source code base which has been used with good results for a number of years. Despite newer versions being released, for these campaigns the version was kept consistent at 3.7.1. The avionics fitted are listed in Table 2 and were chosen for automated long-range flight. A thin iron-on coating was also applied to the aircraft frame to help ensure smooth aerodynamic surfaces, but had an additional effect of increasing the airframes' robustness.

In each aircraft two cameras were mounted in the nose with a forward view. A GoPro Hero 3 (GoPro, San Mateo, CA) camera captured high-resolution video onto on-board storage for postflight analysis. A RunCam Eagle First Person View (FPV) camera was also mounted in parallel, and streamed video to the GCS via a 2.4-GHz wireless link. The live video link proved effective for in-flight visual identification of the plume. A diagram of the 'standard' long-range system is shown in Figure 3a.

The PixFalcon/PixHawk AutoPilot units logged flight data at frequencies between 10 and 50 Hz, including data, such as altitude, airspeed, radio channel output, and Global Position System (GPS) location. A reduced-rate version of the logs could be monitored in real-time from the GCS, and the full logs could be analysed postflight alongside with the recorded videos.

The GCS is comprised of an automated antenna tracker, equipped with a PixHawk hardware board and a two-axis pan and tilt mechanism, and a computer terminal. The antenna tracker automatically maintained alignment between the aircraft and high-gain directional antennas, and provided two of the three links to the aircraft: the telemetry and the FPV video. The computing on-board the tracker consisted of a Raspberry Pi 3 B+. The data from both wireless links were forwarded to a computer terminal via a wired network. The computer terminal ran MavProxy, a custom MavLink Terminal, and modified open-source software (Mission Planner).

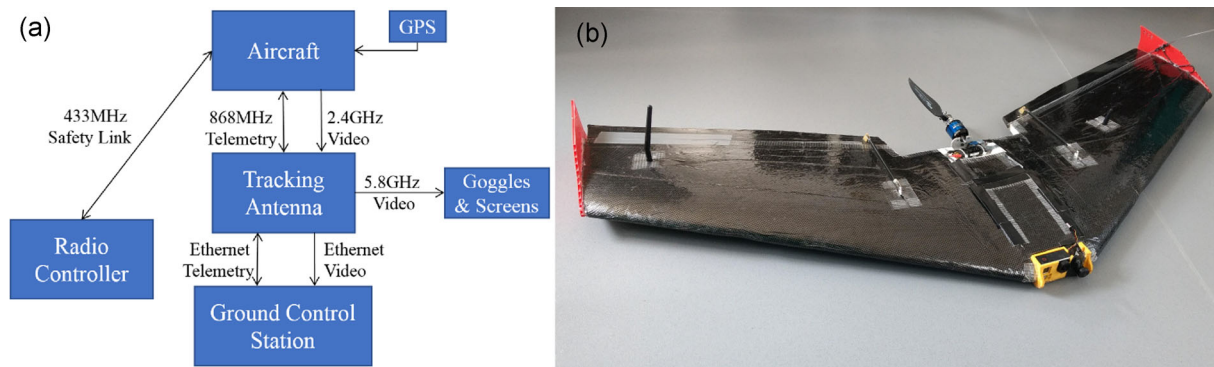


**FIGURE 3** (a) The system diagram for long-range fixed-wing operations, where GPS is Global Position System and GCS is Ground Control Station, and (b) the RiteWing Zephyr II, used to scout the ability of drones to be used at Fuego. No additional sensors were used for the RiteWing Zephyr II flight [Color figure can be viewed at [wileyonlinelibrary.com](http://wileyonlinelibrary.com)]

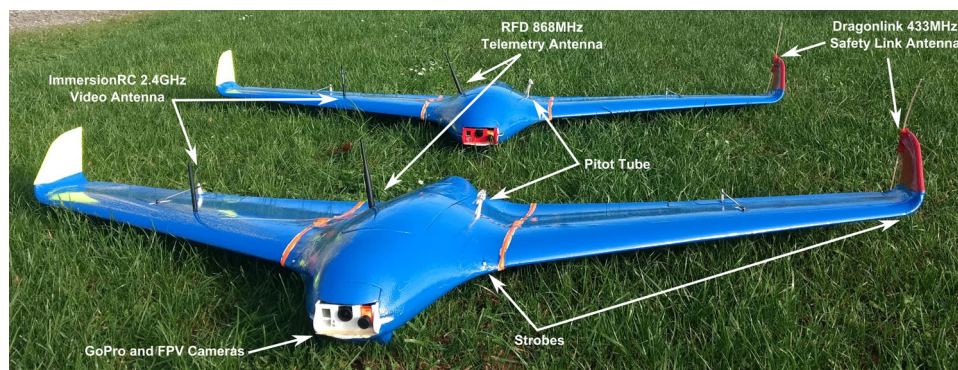


**FIGURE 4** The Skywalker X8 vehicles that were flown in Guatemala, with labels of the main visible external features. Note. The video antennas shown here were used for transport and laboratory testing, and were replaced with skew planar wheel antenna for flight. Sensor placement is discussed in the sensor section below. FPV, First Person View [Color figure can be viewed at [wileyonlinelibrary.com](http://wileyonlinelibrary.com)]

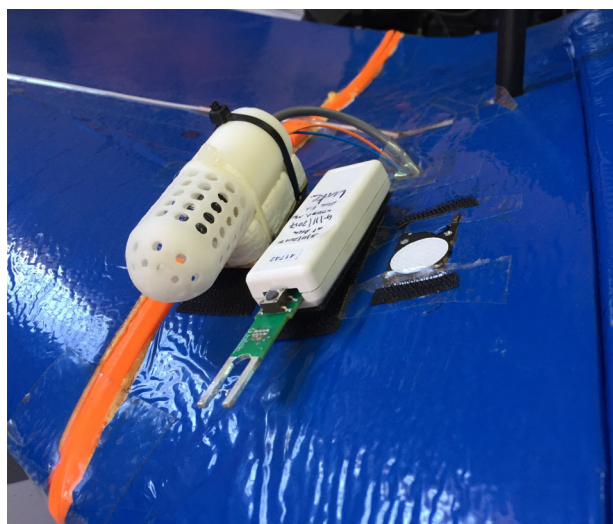


**FIGURE 5** Temperature and relative humidity sensors. The AMP (left) and iMet (centre) sensors mounted externally on one of the Skywalkers. AMP, Avian Meteorological Package [Color figure can be viewed at [wileyonlinelibrary.com](http://wileyonlinelibrary.com)]

## 2.3 | Sensing methods

The methods listed below are for sensing and identifying the plume. The merits of each will be discussed individually as a method for reliably detecting when the aircraft is within a volcanic plume.

### 2.3.1 | Turbulence

The plume is expected to be turbulent relative to ambient air due to the interaction of recently expelled hot ash and gases with the ambient atmosphere. Both the PixFalcon and PixHawk AutoPilot units are fitted with a variety of on-board sensors, which are used and logged by the flight control system. Gyroscopes and accelerometers measure rotation and acceleration around and along each aircraft axis, respectively. Turbulence was sensed by these accelerometers, and to some extent the gyroscopes, however these sensors cannot distinguish plume turbulence from other sources of turbulence, such as clouds.

Properly quantification of turbulence requires specialist devices, such as a five-hole gust probe linked to an accurate, fast-response inertial measurement unit (IMU). These data can then be used to

**TABLE 2** Specifications of the aircraft, based on performance from the missions presented here

Aircraft	RiteWing Zephyr II	Skywalker X8
Maximum achieved flight time	30 min	42 min
Maximum takeoff mass	2.48 kg	4.2 kg
Wingspan	1.4 m	2.1 m
Lithium polymer battery	2 × 4,000 mAh, 14.8 V	2 × 8,000 mAh, 14.8 V
Motor	OS Motor OMA-3820-1200-W	Overlander 5045/10 720 kV and AXi 4120/14 660 kV
Propeller (Aeronaut CAMcarbon)	10 × 6" (folding)	14 × 6" (folding) and 14 × 8" (folding)
Electronic speed controller	Graupner 70 7237.D35	Overlander XP2 80A and Jeti Adv 77 Pro Opto
AutoPilot	Holybro PixFalcon	Unmanned Tech PixHawk
AutoPilot software	ArduPlane 3.7.1	ArduPlane 3.7.1
Safety (pilot) control link	DragonLink V3 Adv (433 MHz)	DragonLink V3 Adv (433 MHz)
Ground Control Station link	RFDdesign 868+ (868 MHz)	RFDdesign 868+ (868 MHz)
Video link	ImmersionRC 700 mW (2.4 GHz)	ImmersionRC 700 mW (2.4 GHz)
Video camera	RunCam Eagle and GoPro Hero 3	RunCam Eagle and GoPro Hero 3

calculate absolute turbulence values using methods such as those presented by Stull (2005). The nature of the operating environment meant these delicate devices would need sophisticated protection measures, which was not conducive to minimising the equipment required to sense the plume. Fortunately, vertical (Z-axis) acceleration is sensed by the IMU in the flight computer and is sufficiently representative of turbulence for the plume identification attempted here. These data could easily be incorporated into an on-board detection system as no additional mass or significant computing power would be involved.

### 2.3.2 | Temperature and relative humidity

As the plume reaches maximum altitude soon after eruption, the plume as a large entity becomes neutrally buoyant. This means that as an entire body the temperature within it is no longer significantly higher than that of the surrounding air. If the plume is flown through after this stage it is likely that any temperature change measured would be minimal. Volcanic emissions from Fuego originate from the subduction zone off the coast of Guatemala in the Pacific Ocean, which could lead to a humid plume upon expulsion into clear air. It is likely that this will vary with distal range (from the summit). If there is a significant change in either temperature or relative humidity upon entering the plume then this could be included into the plume-detection system with relative ease, because temperature and relative humidity (Temp/RH) sensors are often small and have low power requirements.

Two types of Temp/RH sensor were used, both of which are described below. One is available to buy commercially and the second was developed by a member of the team.

#### *iMet-XQ, manufactured by International Met Systems*

The sensor contains a GPS unit, bead thermistor, capacitive RH sensor, and piezoresistive pressure sensor, logging at 60 Hz. The

manufacturer's specifications are given in Table 3. This was mounted inside the nose of the aircraft, with the sensor tips in the airflow entering the aircraft, or externally on the forward section of the fuselage.

#### *Avian Meteorological Package*

The Avian Meteorological Package (AMP) is a modified version of the Eagle Sensor Package (ESP) as described by R. M. Thomas et al. (2018) and Greatwood et al. (2017). The ESP evolved to use an Atmel M0 (Atmel, San Jose, CA) cortex chip on a commercially available microcontroller (Adafruit Feather), and a daughter board was constructed containing a GPS chip, accelerometers, magnetometers, BMP280 pressure sensor, the fast tip, and I<sup>2</sup>C connections for the P14 rapid RH sensor, which were all logged at 5 Hz.

The AMP used here is an alternative to the iMet, with greater flexibility for additional sensors and integration with UAV systems. To ensure the sensors were in the best airflow possible, without creating disproportionate amounts of drag, it was mounted on the upper surface of the fuselage near the leading edge. The specifications are given in Table 4. Although the AMP is pending validation for sensing of absolute values, the data collected qualitatively show its potential use.

**TABLE 3** iMet-XQ sensor specifications

	Sensed parameter		
	Humidity	Temperature	Pressure
Sensor type	Capacitive	Bead thermistor	Piezoresistive
Range	0–100% RH	–95°C to +50°C	10–1,200 hPa
Response time	5 s at 1 m/s	2 s	10 ms
Accuracy	±5% RH	±0.3°C	±1.5 hPa
Resolution	0.7% RH	0.01°C	0.02 hPa

**TABLE 4** Avian Meteorological Package (AMP) sensor specifications (Greatwood et al., 2017)

	Sensed parameter		
	Humidity	Temperature	Pressure
Sensor ID	IST P14 Rapid	GE Fastip	Bosch BMP280
Sensor type	Capacitive	Glass bead thermistor	MEMS
Range	0–100% RH	–30°C to +40°C	300–1,100 hPa
Response time	<1.5 s	0.1 s	5.5 s
Accuracy	±<0.75% RH	±0.2°C	±1 hPa
Resolution	0.10% RH	1°C	0.01 hPa

Abbreviation: RH, relative humidity; MEMS, microelectromechanical systems.

### 2.3.3 | Visual cameras

Visual identification of the plume is possible using standard RGB cameras. Set to record at a resolution of 1,920 × 1,080 pixels, the GoPro Hero 3, fitted in the nose of both aircraft types, was used to assess whether the UAV was in the plume. Upon approaching the plume, the darker ash cloud took up an increasing proportion of the frame, and the relative enormity of the plume compared to the UAV meant if the aircraft entered the plume the image changed colour completely. This was most clearly seen by comparing the colour of a ‘constant’ object (such as distant sky or clouds) at a point when the aircraft is known to be in clear air with various points going into and out of the plume.

The GoPro Hero 3 provides a good qualitative indicator of plume interaction, however real-time image processing requires significant computational resources. While increasing on-board computing power is possible, it minimises the remaining payload available for scientific instrumentation and is therefore undesirable. It was instead used as a method of verifying the data collected by the accelerometers and Temp/RH sensors.

### 2.3.4 | SEM ash-collection stubs

Secondary Electron Microscopy (SEM) stubs are a widely accepted way of collecting ash samples in the volcanological community, and were used here as a way of verifying flight through the plume while using the other methods listed in this section. The stubs are metallic and collect ash on a sticky flat disc measuring 12.5 mm in diameter, have an 8-mm stem for handling, and weigh approximately 1 g each. They must be analysed postflight in a laboratory environment so they are not possible to incorporate with a real-time detection system.

A customised ash-collection unit was created for mounting the SEM stubs on the vehicle in a position exposed to the airflow. A servo-operated cover allowed the stubs to be isolated during takeoff, climb/descent, and landing to prevent contamination, and was controlled manually by the operator from the GCS. Mounted on the floor at the rear of the payload bay in the Skywalkers, this unit sat in the airflow proud of the main hatch.

## 3 | IN-PLUME-DETECTION METRIC

The following metric was developed for real-time plume sensing:  $t$  is the flight time in seconds,  $alt$  is the altitude in metres AMSL,  $absH$  is the absolute humidity,  $relH$  is the relative humidity, and  $z$  is the Z-axis vertical acceleration in  $m/s^2$ .  $P_{inPlume}$  in Equation (1) represents the probability of the aircraft being in a plume.

$$P_{inPlume} = \begin{cases} C_{inPlume}, & C_{inPlume} < 1, \\ 1, & C_{inPlume} \geq 1, \end{cases} \quad (1)$$

$$C_{inPlume} = C_{alt} \cdot C_{absH} \cdot (C_{accZ} + C_{relH}), \quad (2)$$

where  $C$  represents the components of the formula, the individual definitions of which are defined in Equations (3)–(6).  $alt$  is the GPS altitude AMSL,  $absH$  is the absolute humidity,  $z$  is the Z-axis acceleration, and  $relH$  is the relative humidity.

$$C_{alt} = \begin{cases} 0, & alt < 3860, \\ 1, & alt \geq 3860, \end{cases} \quad (3)$$

$$C_{absH} = \begin{cases} 0, & absH > 4.95, \\ 1, & absH \leq 4.95, \end{cases} \quad (4)$$

$$C_{accZ} = \begin{cases} 0, & i \leq 0, \\ \sqrt{\frac{1}{500} \sum_{n=i}^{500+i} (z_i - \mu)^2}, & i > 0, \end{cases} \quad (5)$$

where

$$i = 50(t - 10) \quad \text{and} \quad \mu = \frac{1}{500} \sum_{n=i}^{500+i} z_i,$$

$$C_{relH} = \frac{relH_t - \min\{relH_j^{7200+i}\}}{50}, \quad (6)$$

where

$$j = 60(t - 120).$$

This initial plume-detection metric was developed during the postprocessing of the flight results, and makes the following assumptions:

- The plume maintains near-constant altitude in the flight area around Fuego, such that a lower altitude limit of 3,860 m AMSL can be imposed.
- The absolute humidity of the plume is below 4.95 g/m<sup>3</sup>, which it was on all the processed occasions.
- The standard deviation of the accelerometer data over the past 10 s (500 points at 10 Hz) is a reasonable indicator of turbulence levels.
- The difference between the current relative humidity and the minimum value of relative humidity in the last 2 min (7,200 points at 60 Hz) is a reasonable indicator of local data peaks.



## 4 | FLIGHT RESULTS

A total of 19 flights reached altitudes over 1,900 m AMSL across the three trips, with 11 reaching plume altitude or above. Meteorological conditions were best in the morning with rapid deterioration limiting useful operating time and often requiring early return of the aircraft. Four key flights were chosen for analysis here, each having intersected the plume independently. Details of these flights are given in Table 5.

Supporting Information Material has been submitted alongside this paper, containing video from each flight. This video further reinforces the evidence of UAV/Plume interaction given here. Details of this material are given in the appendix.

Volcanic activity during Flight A involved discrete plumes similar in shape visually to cumulus clouds, with a cloud layer significantly below summit altitude and some high-altitude clouds significantly above summit altitude. Flights B and C took place when the volcano's behaviour was significantly different; it was producing constant streams of ash-filled plume with no clear breaks. There was a significant amount of cloud during Flight B, however the UAV climbed out of it at 2,612 m AMSL and descended back into it at 2,727 m AMSL, some 1,000 m below plume-interception altitude. Although there was some localised cloud on the summit, the UAV was in clear air when it flew through the plume. Images from Flight C show cloud gathering on the windward side of Fuego, however they stayed there during the course of the flight due to local weather patterns. Flight C was conducted without flying through or above any cloud. Flight D took place with small eruptions giving off a large, variably dense, ashy plume every 1–4 min. There were no clouds present during Flight D. The prevailing (North Easterly) wind conditions were present for Flights A–C. The wind for Flight D was from a Southerly direction, which meant interception of the plume could only happen at a proximal point. Distal interception would have meant losing line of sight communications with the UAV. The points at which the aircraft flew through the plume are marked in Figure 6.

### 4.1 | Flight A

The initial flight plan was chosen after a series of software-in-the-loop simulations. After a manual launch the aircraft entered

automated flight and climbed towards the summit for a short distance. It then entered a 300-m diameter climbing spiral to 4,000 m AMSL before continuing in a straight climb towards a waypoint at 4,100 m AMSL, 500 m from the crater. The descent was direct from the turn point to a point near the GCS, where it then entered a controlled spiralling descent before landing manually.

Climbing in a spiral is inefficient because lift is lost proportionally to the cosine of the roll angle, however this plan maximised time on the level approach towards the summit and the proximity of the climb to the GCS meant progress could easily be monitored. The volcano erupted approximately 12 min into the flight and the alignment of the flight path with the wind (average headwind of 7 m/s) meant the plume was intercepted during the gradual climb from 4,000 to 4,100 m AMSL, approximately 1.9 km from the summit.

Figure 7 shows frames from the on-board forward-facing video. Frame (b) for this flight shows being in, and a little below, the estimated centre of the plume. Figure 8 shows some of the flight logs from Flight A.

The timings of the video agree with the logs in Figure 8, indicating a plume intersection at around 14 min and 45 s into the flight. It is clear from both the video and the Z-axis acceleration logs that the turbulence experienced in and after the nominal plume point is significantly more than in clear air.

### 4.2 | Flight B

The data presented here are from the first of two important flights in November 2017 and indicate intersection with the plume using the autopilot sensors, GoPro camera, Temp/RH mounted as shown in Figure 5, and ash collection. This is significant for the development of automated plume detection using UAVs.

The bearing and altitude of the plume were estimated using ground measurements, then the flight plan designed so that a large cross-wind area was covered to maximise the chance of plume interception. The aircraft climbed to altitude in a spiral before a gradual straight-line climb, then traversed across the estimated bearing of the plume. It then turned and followed the same track in reverse to return to the GCS. This gave the on-board camera a good view of the approach to the plume, making comparison of frames around the plume straightforward. Using the FPV video as a guide,

**TABLE 5** Flight details

	Flight			
	A	B	C	D
Aircraft	Zephyr II	Skywalker X8	Skywalker X8	Skywalker X8
Date	20 Feb. 2017	6 Nov. 2017	7 Nov. 2017	11 Oct. 2018
Local takeoff time (am)	11:40	11:35	07:56	06:10
Flight duration (min)	29:45	40:34	41:17	37:51
Max. altitude AMSL (m)	4,089	3,920	4,082	4,410
Battery used (mAh)	6,575 (82%)	9,652 (60%)	12,458 (78%)	10,880 (68%)
Avg. flight airspeed (m/s)	20 (GPS)	20	20	26

Abbreviations: AMSL, Above Mean Sea Level; GPS, Global Position System.



**FIGURE 6** Google Earth (2018) image showing the plume-interception points over the four chosen flights, relative to the Observatory and Summit. Flight paths have not been shown to maintain clarity regarding the true location of interceptions [Color figure can be viewed at [wileyonlinelibrary.com](http://wileyonlinelibrary.com)]

the ash-collection unit was opened after the straight-line climb was complete and was closed at the same point upon return, immediately before the descent started. The plume was transected approximately 5.7 km from the summit.

Figure 7 shows three frames from the forward-facing video, corresponding to points before, during, and after plume intersection. Note the differences in colour between (a) and (b), and then again between (b) and (c). In all these frames Fuego's summit was in cloud, located near the intersection of the horizon and right-hand side of the image.

Flight logs from Flight B are shown in Figure 9, where two distinct periods of turbulence can be seen. These two sections correspond to the outbound and return paths of the UAV through the plume. Ash of a significant size was collected on this flight, some of which is shown in Figure 10.

The Temp/RH sensor on-board for this flight was the iMet-XQ, the results of which are shown in Figure 11. These data have been aligned with flight time using GPS time. The climb and descent both went through cloud, saturating the humidity sensor.

$P_{InPlume}$  was calculated in postprocessing at time intervals of 50 Hz for this flight, the results of which are shown in Figure 12, below the plot of selected normalised flight data.

### 4.3 | Flight C

The sensing methods on-board this flight were the autopilot sensors, GoPro Hero 3 camera, and both Temp/RH sensors mounted as shown in Figure 5. The wind shear on this day was significant, with larger eruptions pushing the plume to a greater altitude where they were caught by a Southerly wind. Lower-level eruptions would instead be caught by a different wind layer and travel on a bearing of approximately  $260^\circ$ , and it was this plume that was aimed for and

flown through. The wind speed along this section was approximately 13 m/s according to the flight logs. The throttle, pitch, and Z-axis acceleration logs are shown in Figure 13.

In Figure 7a the lower plume is parallel to the horizon to the left of Fuego, and the higher plume is visible above the summit moving to the right. Image (b) was taken before the turn into the wind. The haziness between the aircraft and summits of Fuego (foreground) and Acatenango (background) is the plume. Image (c) is from just before the aircraft turned away from the wind, and shows more haziness at the level of the aircraft.

Instead of transecting the plume, the flight plan met the estimated plume bearing and then turned towards the summit before returning to the GCS. The section of the flight that was on a bearing directly towards Fuego went from a distance of 5.7–3.9 km from the crater, at the end of which the plume was flown through. Once again the altitude of the plume proved extremely hard to estimate. The data show that during this flight the aircraft started above the plume by some estimated 100 m and descended into it as it approached the summit as it went from 4,080 to 4,014 m AMSL.

The iMet-XQ was fitted alongside the AMP for this flight, the results of which are shown in Figure 14.

$P_{InPlume}$  was calculated in postprocessing at time intervals of 50 Hz for this flight, the results of which are shown in the lower part of Figure 15.

### 4.4 | Flight D

This flight overflew the crater, loitered a short distance from the summit, and then flew through the plume before returning to the GCS (Figure 16). The plume intersection was flown in FBW mode, where the autopilot maintains wings-level flight but the pilot has control of throttle, pitch, and roll (from level). The sensors on-board

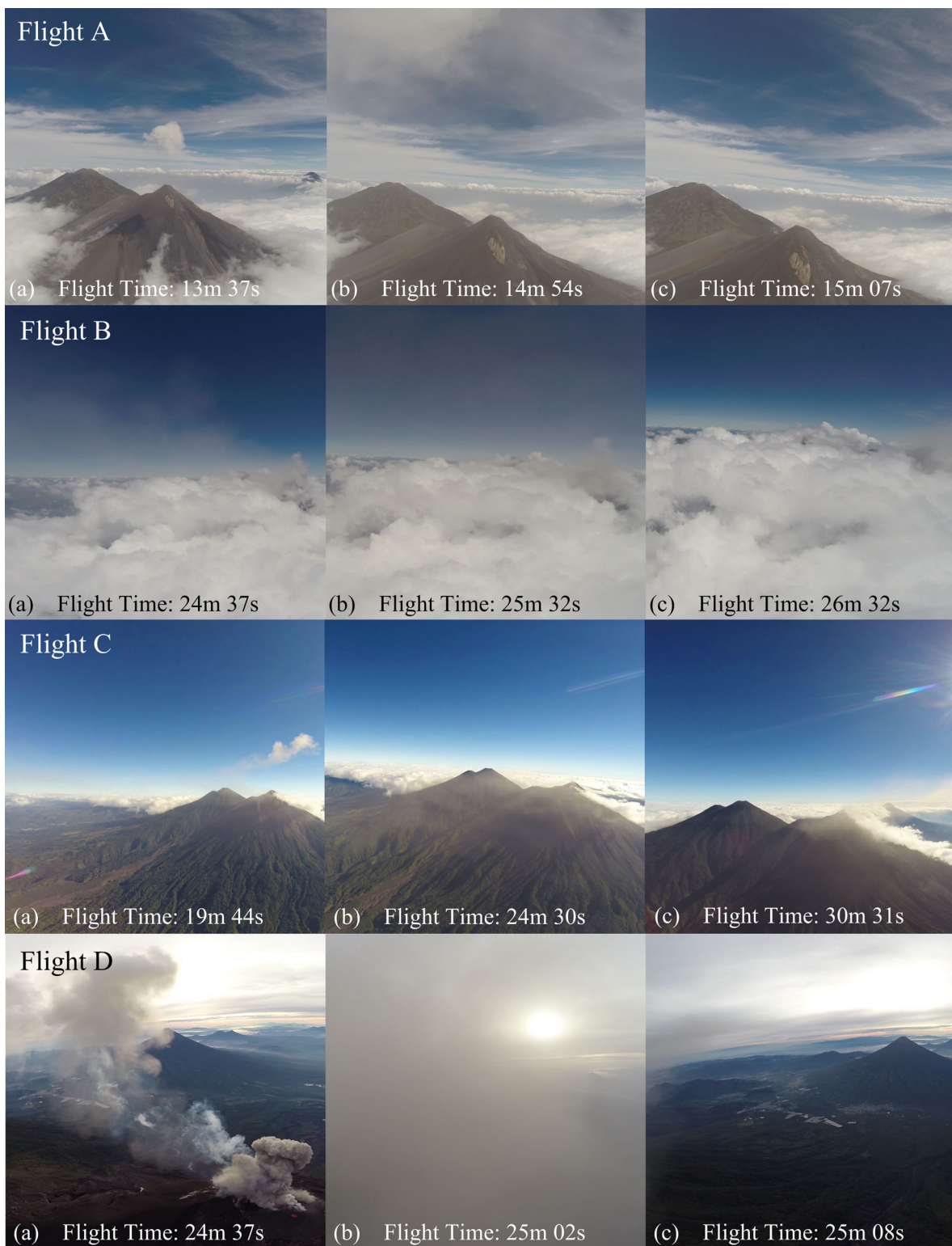


**FIGURE 7** Frames from on-board video for Flights A, B, and D show (a) before, (b) during, and (c) after plume interception. The frames for Flight C show (a) before, (b) approaching, and (c) during plume interception. Note the differences in colour and change in plume location between frames [Color figure can be viewed at [wileyonlinelibrary.com](http://wileyonlinelibrary.com)]

were the autopilot sensors, GoPro Hero 3 camera, and both Temp/RH sensors. The AMP was mounted on the wing as in Figure 5 but without the white protective shield, and the iMet-XQ was mounted in the nose, protruding from just above the FPV camera. These results

are shown in Figures 17 and 18. The plume was intercepted approximately 0.5 km from the crater centre. A temperature increase of approximately 2°C was recorded on the iMet, and the relative humidity showed a spike of around 10%.

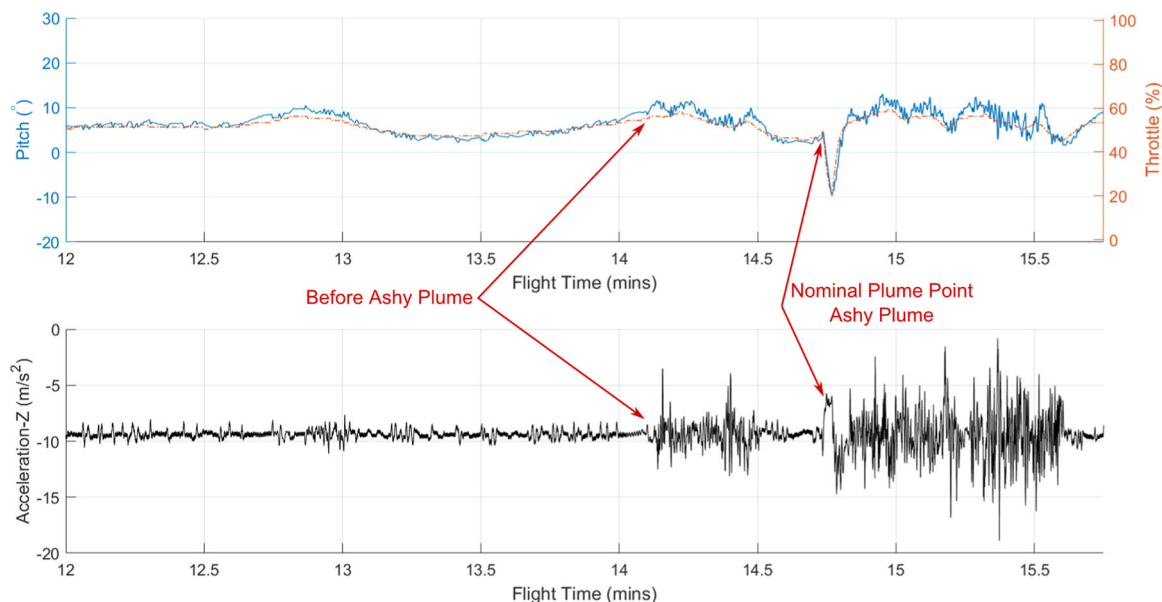


**FIGURE 8** Flight logs of the Zephyr II showing flight through the plume; pitch (top, blue, solid), throttle (top, orange, dot-dash), and vertical acceleration (bottom, black, solid). A significant increase in activity just after 14 min of flight indicates initial plume interception [Color figure can be viewed at [wileyonlinelibrary.com](http://wileyonlinelibrary.com)]

The aircraft climbed in straight legs to minimise the loss of lift in the constant turn, then loitered near the summit until a suitable ash cloud was released. FBW mode was then activated, and the aircraft was manoeuvred through the plume with minimal change in pilot control inputs during the fly-through section of flight (pink section in Figure 16). The aircraft was then returned to automated flight for the return to the GCS.

$P_{InPlume}$  was calculated in postprocessing at time intervals of 50 Hz for this flight, the results of which are shown in the lower part of Figure 19.

## 5 | PLUME DETECTION AND FLIGHT ANALYSIS

In this paper the sensing and identification of volcanic plumes using fixed-wing UAVs is considered. A volcanic plume is the mixture of gases and ash emitted by an eruption, however for sensing purposes the boundary is hard to define, with gases diffusing at different rates and the only visible part being the ash. In this section we will review the data from the on-board sensors showing that the UAVs interacted with plumes on a number of occasions, and assess the accuracy of the hypothesis.

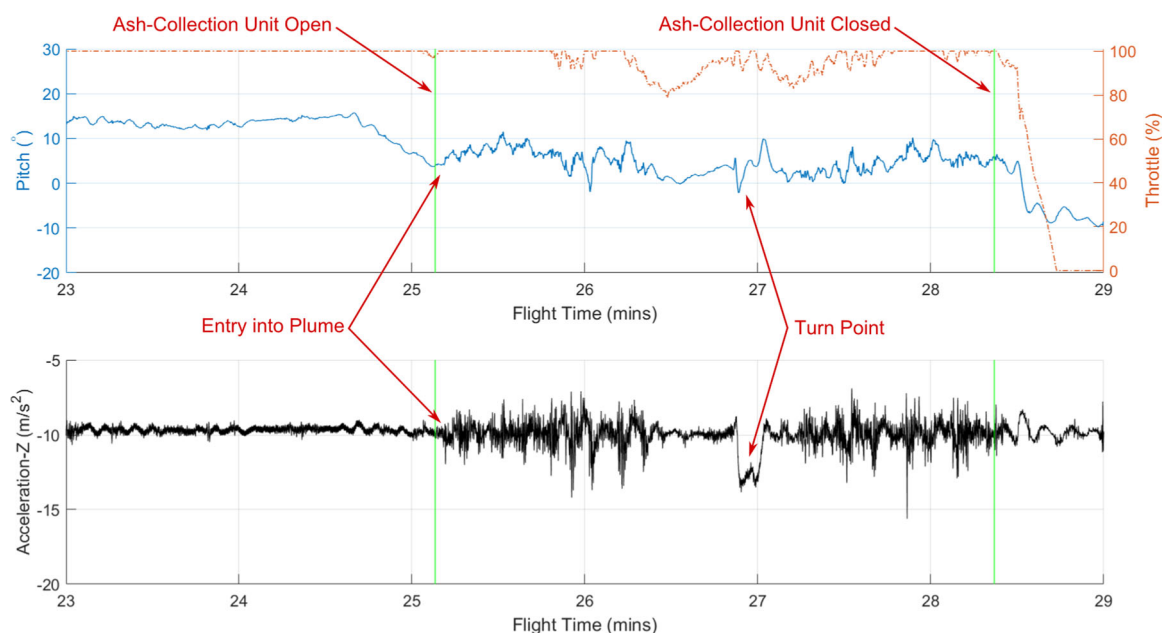


**FIGURE 9** Flight logs of a Skywalker showing flight through the plume; pitch (top, blue, solid), throttle (top, orange, dot-dash), ash-collection unit open/close points (green, vertical, solid), and vertical acceleration (bottom, black, solid) [Color figure can be viewed at [wileyonlinelibrary.com](http://wileyonlinelibrary.com)]



**FIGURE 10** Results from the SEM stubs, showing ash collected during Flight B. SEM, Secondary Electron Microscopy

Autopilot Pitch ( $^{\circ}$ ), Throttle (%), and Z-axis acceleration ( $m/s^2$ ) are shown here because they can indicate a variety of different phenomena. The Total Energy Control System (TECS) flight controller works on balancing potential and kinetic energies, responding to errors in predictable ways as indicated in Table 6.

The responses in Table 6 equate to a required increase or decrease in lift, compensating for a decrease or increase in lift, respectively. There are a number of parameters that can effect lift generation, the most effective being airspeed.

Turbulent air was expected upon entering the plume, with a higher density than ambient air. The turbulence felt in the plume is caused by the circulation of hotter air rising to the top of the plume and cooling, before sinking down again. The average temperature in the plume must be equivalent to the ambient temperature, else buoyancy would not be neutral. The centre of the plume is expected to be roughly equivalent to ambient air temperature, whereas the bottom is expected to be warmer and the top is expected to be cooler.

An increase in the activity and magnitude of Z-axis acceleration indicates turbulence, with increased high-frequency activity in the pitch data too. A discrete increase in air density would see a response from the TECS controller, equivalent to being above the target altitude. Changes in wind speed also cause a response,

however they tend to be gradual therefore causing nondiscrete responses.

This section will consider each flight in turn, discussing the flight in general and, more specifically, the detection of the volcanic plume during the mission. Data collected by sensors on-board each flight will be considered and compared. It should be noted that the Skywalker flown for Flight B and Flight C was fitted with a motor that was not suited to the mission profile flown. The cruise throttle was near 100%, leaving little excess thrust for efficient climbing. The motor was replaced before Flight D, hence the significant change in cruising throttle setting.

## 5.1 | Flight A

The camera (Figure 7) showed that the aircraft flew through the lower section of the plume front at a flight time of approximately 14.75 min, and the accelerometer data (Figure 8) showed a corresponding increase in activity. The aircraft hit a patch of turbulent air approximately 30s before reaching the ash-rich plume, likely a nonvisible part of the plume that was released in the degassing before the main ashy eruption. The accelerometer data indicate an upwards acceleration and a corresponding reduction of pitch and throttle at the Nominal Plume Point, which combined suggest a sudden increase in lift due to the increased density of the plume.

A high level of turbulence continued over the following minutes of flight; the flight logs in Figure 8 showed relatively smooth flight before reaching the plume, however after passing through the plume the aircraft continues to move through turbulent air for over 60s (a distance of 1.26 km at 21 m/s). This plume 'tail', or wake, agrees with what is known about plumes through oblique photogrammetry experiments (U.S. Department of Interior, 2013).

The turbulence experienced by the Zephyr II in the plume was 1.9 km from the summit and was easily distinguishable in the logs. It decided after this flight that Temp/RH sensors would be beneficial for further identification of the plume, only adding a small mass to the system. Real-time processing of this turbulence data can be moved on-board, however alone it will not suffice as a method for sensing the plume because turbulence can also be encountered in nonplume environments, such as clouds.

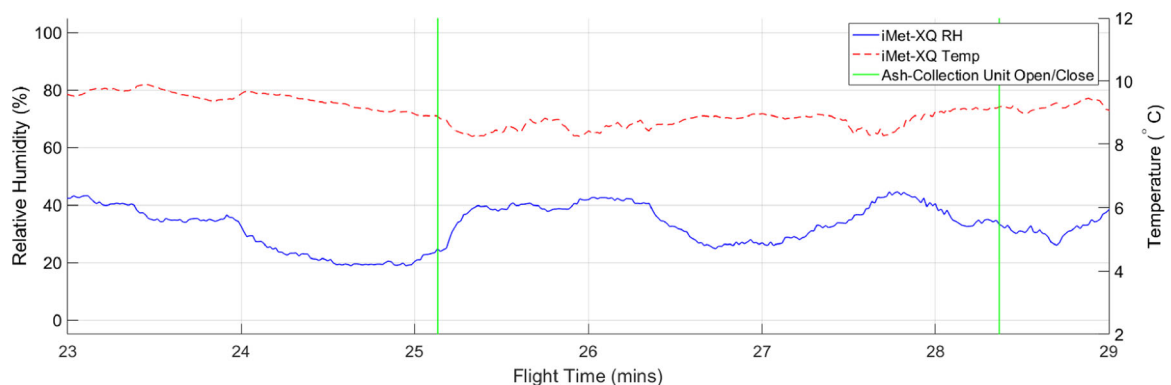


**FIGURE 11** Results from the iMet-XQ sensor on Flight B, showing temperature (red, dashed) and relative humidity (blue, solid). The vertical green lines indicate the ash collector open/close times, as in Figure 9 [Color figure can be viewed at wileyonlinelibrary.com]

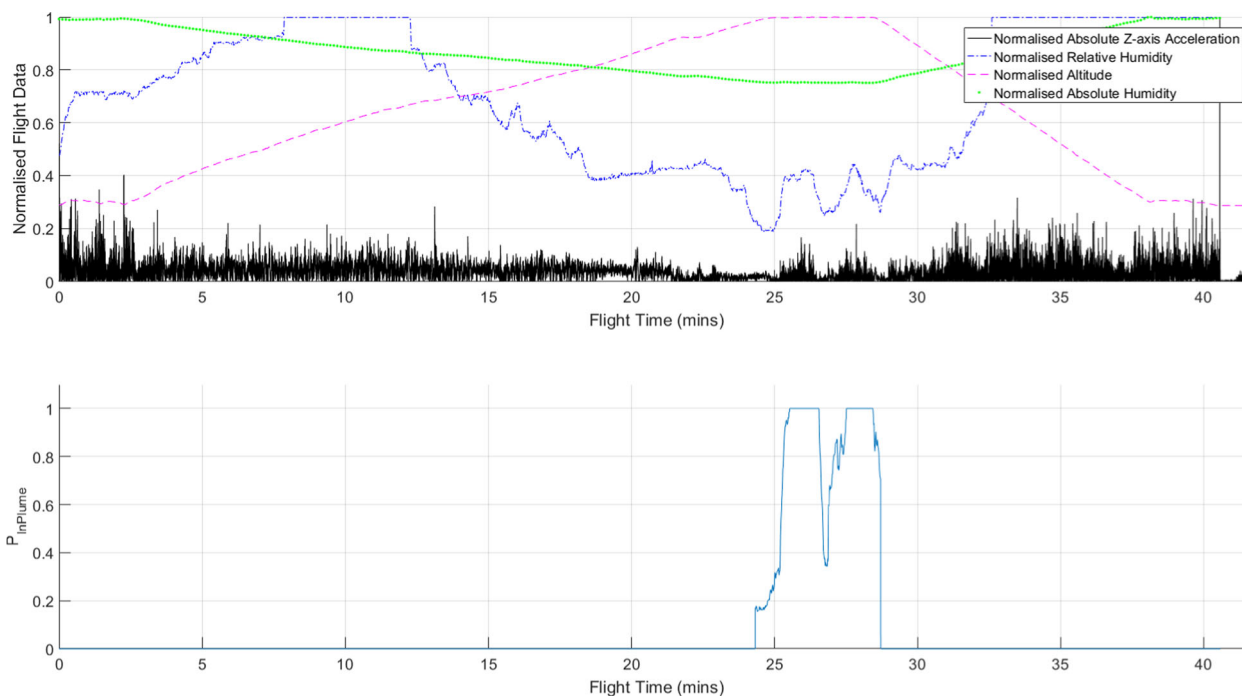


**FIGURE 12** Normalised flight performance metrics (top) and  $P_{InPlume}$ , calculated using Equation (1) (bottom). The metric aligns with increased turbulence (black), local relative humidity spikes (blue), and with the video, showing two plume interceptions between 25 and 28 min flight time [Color figure can be viewed at [wileyonlinelibrary.com](http://wileyonlinelibrary.com)]

## 5.2 | Flight B

Key to this flight was the evidence collected by the ash-collection unit. The altitude and FPV video were used as indicators for when to open the unit, and was closed at the same point on the return journey. These points are indicated in Figure 9 by the vertical solid

green lines. The particulates on the SEM stubs were analysed in a laboratory and there was a significant and confirmed presence of ash on both stubs, some of which is shown in Figure 10. The volcanological implications of these collections will be discussed in a separate publication.

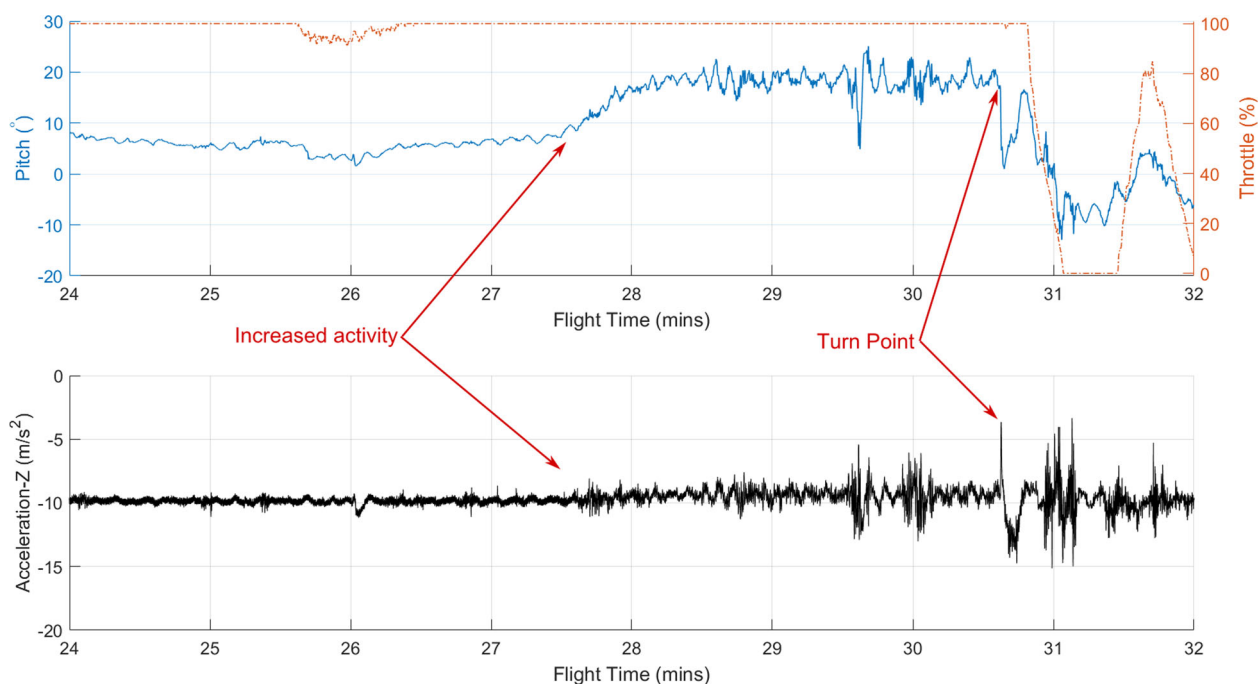


**FIGURE 13** Flight logs of a Skywalker showing flight through the plume; pitch (top, blue, solid), throttle (top, orange, dot-dash), and vertical acceleration (bottom, black, solid). The summit-approach leg started around 26 min, where the throttle dips below 100% [Color figure can be viewed at [wileyonlinelibrary.com](http://wileyonlinelibrary.com)]

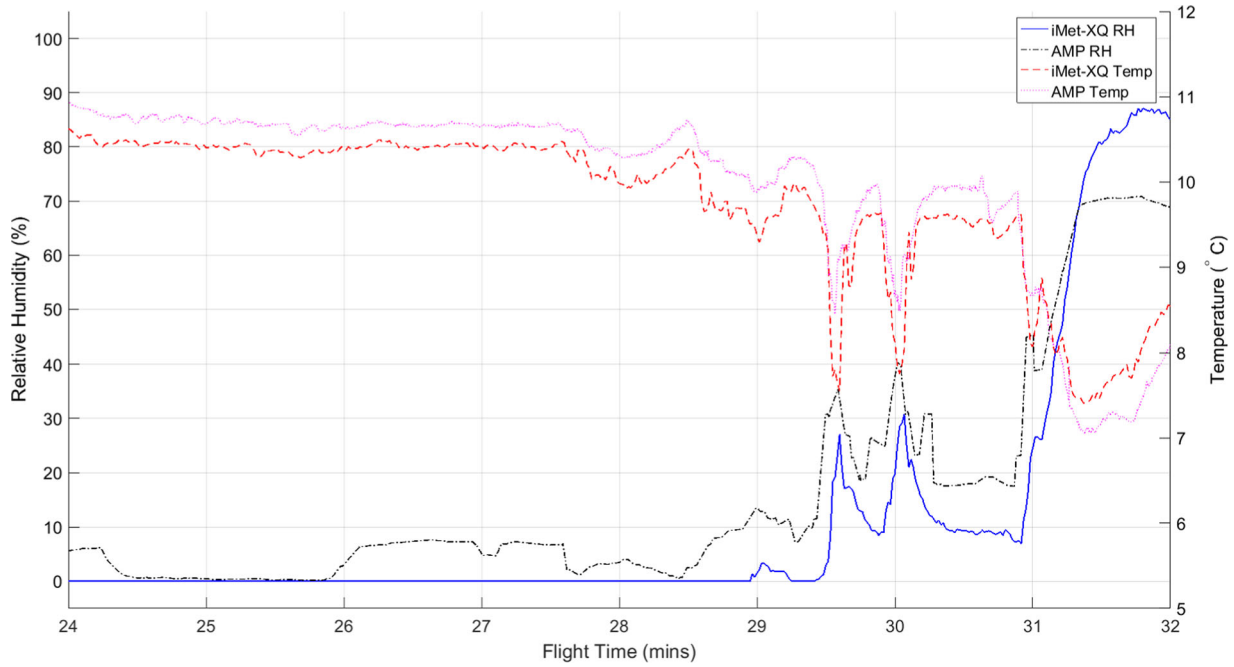


**FIGURE 14** Results from both Temp/RH sensors on Flight C. Note the drop in Temp at the same time the RH peaks. AMP, Avian Meteorological Package; RH, relative humidity [Color figure can be viewed at wileyonlinelibrary.com]

Regarding the flight log plots in Figure 9, there are two distinct periods of increased turbulence during the period of interest. The first corresponds to the initial pass through the plume, and the second corresponds to the return path after the turn. Peak turbulence was encountered centrally to these sections.

From around 25.75 min flight time the throttle starts to fluctuate, which along with a reduced pitch angle suggests excess lift is being

generated. Again, this is a suspected result of the slightly increased density in the plume.

Figure 11 shows no significant change in temperature during the plume interception, suggesting that the UAV flew relatively close to the centre. The relative humidity is approximately 20% either side of the plume, but goes to approximately 40% on each of the plume interceptions. The humidity either side of the plume is the lowest

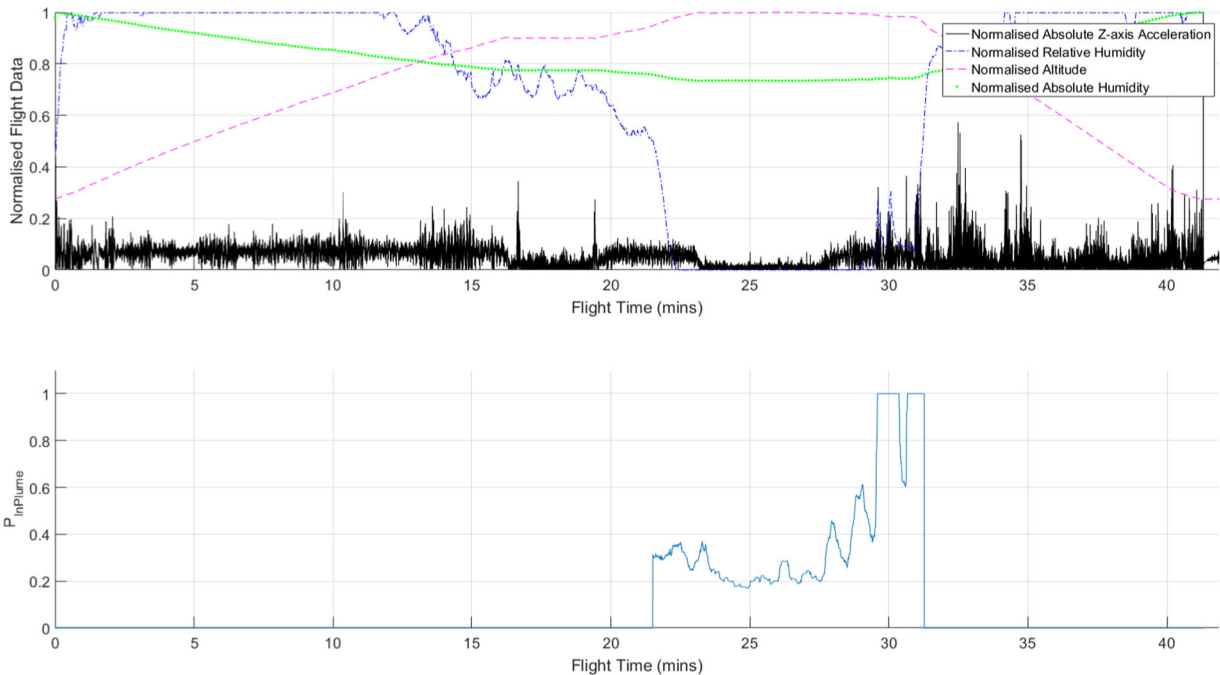


**FIGURE 15** Normalised flight performance metrics (top) and  $P_{InPlume}$ , calculated using Equation (1) (bottom) [Color figure can be viewed at wileyonlinelibrary.com]

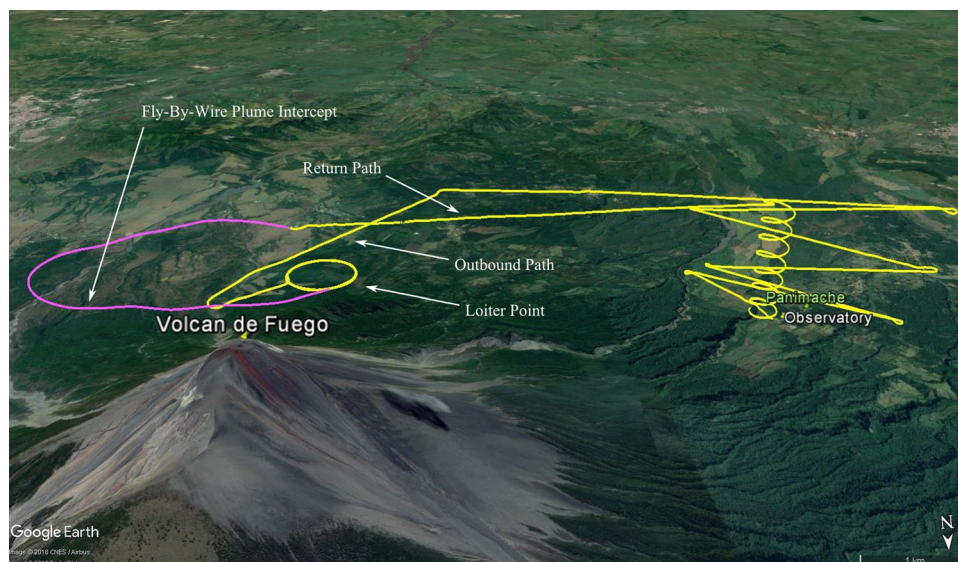


**FIGURE 16** Skywalker flight-path from Flight D shown on Google Earth (2018), with key tracks and locations labelled. Note the Fly-By-Wire section near the summit (pink), where pilot control of the aircraft manoeuvred it through the proximal plume [Color figure can be viewed at [wileyonlinelibrary.com](http://wileyonlinelibrary.com)]

recorded on this flight. The climb and descent on this flight were through cloud, saturating the RH sensor. It was calculated that the UAV climbed out of the atmospheric boundary layer at 24 min flight time, approximately 200 m below the altitude of the plume. As shown in Figure 11 the boundary layer was at similar RH levels to the plume, which means if the plume was encountered below the boundary layer then it could be indistinguishable from ambient air using RH data alone.

### 5.3 | Flight C

Figure 7 shows three frames from the flight video. The aircraft started the approach leg above the plume, which meant the

background features in the video were ground and volcano, not clear sky. Considering the camera alone, it is not clear that the plume was flown through. The other sensors indicated a plume interception towards the end of the summit-approach leg.

Pitch and Z-axis acceleration data in the flight logs (Figure 13) suggest an increasing amount of turbulence from approximately 28 min flight time until the turn point. At 26 min flight time the pitch is at a near-zero value, and the throttle setting was approximately 90%, indicating that the aircraft reached the required altitude at the turn onto summit-approach. The throttle remains at 100% to maintain airspeed, and then the pitch increased to approximately 20°. The aircraft is attempting to climb over this period (Table 6),

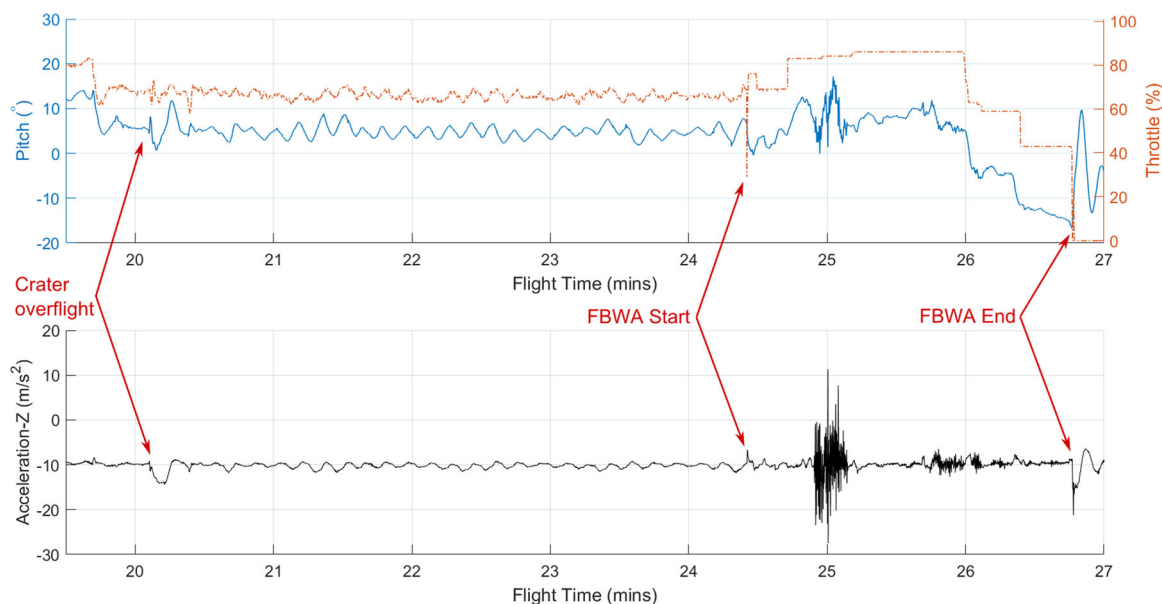


**FIGURE 17** Flight logs from Flight D showing flight through the plume; pitch (top, blue, solid), throttle (top, orange, dot-dash), and vertical acceleration (bottom, black, solid). The aircraft was in Fly-By-Wire mode, with manual control over the throttle [Color figure can be viewed at [wileyonlinelibrary.com](http://wileyonlinelibrary.com)]



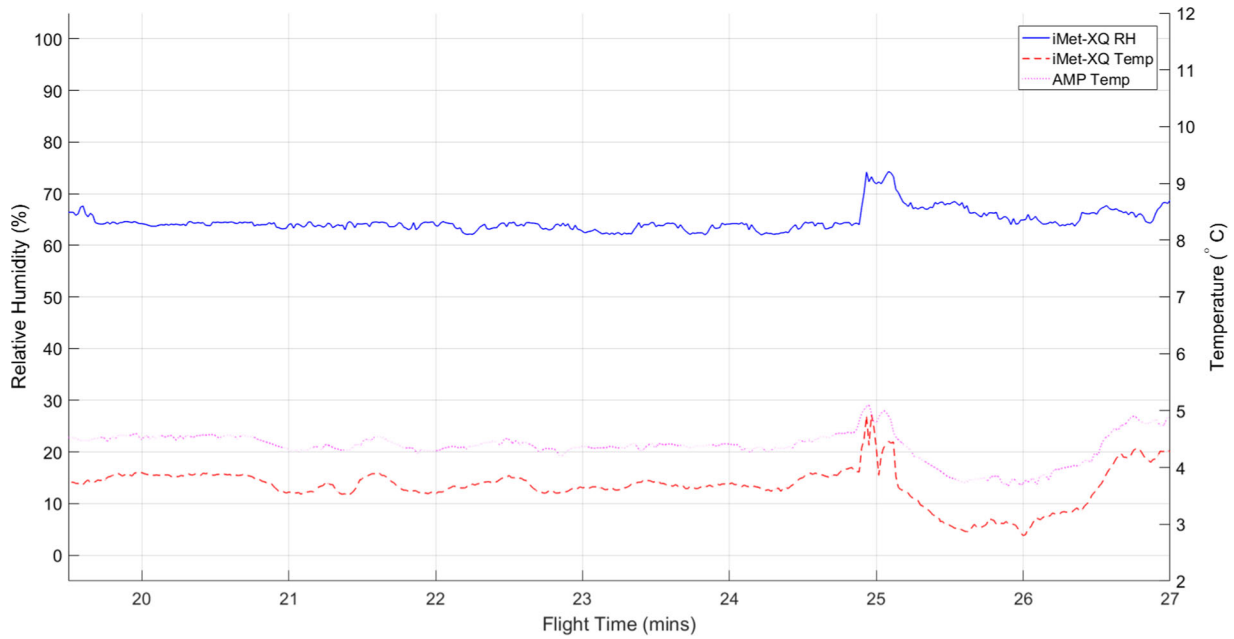


**FIGURE 18** Results from both Temp/RH sensors on Flight D. There is a peak in both Temp and RH in the plume. The AMP RH data are not presented here due to an uncalibrated sensor. AMP, Avian Meteorological Package; RH, relative humidity [Color figure can be viewed at wileyonlinelibrary.com]

however we know that it actually descends until it reaches the turn point.

Temp/RH data (Figure 14) show some differences between the iMet and the AMP. Outside this plot the iMet RH saturates in the cloud on the ascent and descent, and registers 0% during the summit-approach leg, the AMP peaks at around 85% and is mostly nonzero during the approach leg. One explanation for the lack of saturation

on the AMP is the large protective shield fitted for protection of the delicate sensors, as seen in Figure 5. There are two peaks in RH, at 29.6 and 30.1 min, which correspond to Temp drops of 2°C and increased Z-axis acceleration. These plume points indicate UAV/Plume interaction. Relative humidity registered at near 0% before the section of turbulence, and slowly increases up to 29.5 min. At the plume points the RH is approximately 30%, and drops down to 10%

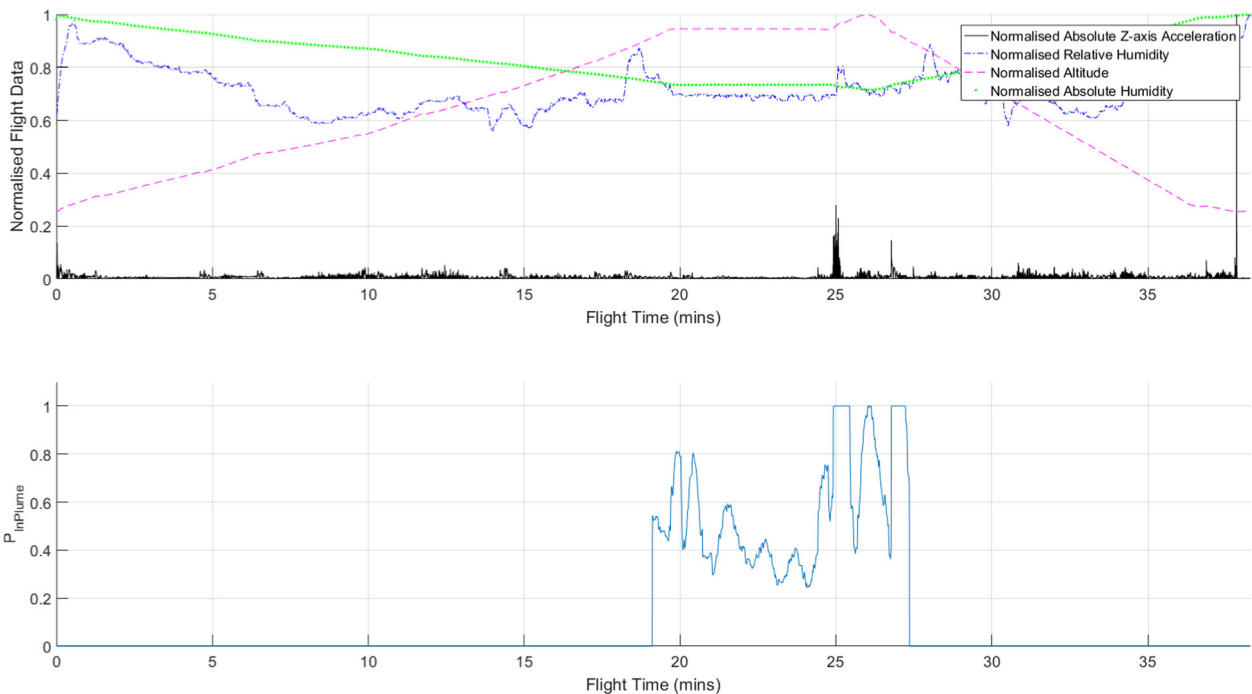


**FIGURE 19** Normalised flight performance metrics (top) and  $P_{InPlume}$ , calculated using Equation (1) (bottom) [Color figure can be viewed at wileyonlinelibrary.com]

**TABLE 6** TECS behaviour

Error	Response
High airspeed	Throttle down, pitch up
Low airspeed	Throttle up, pitch down
Above target altitude	Throttle down, pitch down
Below target altitude	Throttle up, pitch up

Abbreviation: TECS, Total Energy Control System.

again before the aircraft turns at the end of the leg. RH for Flight C was similar to Flight B, at a point of turbulence that was similar both in relative increase and magnitude. The Temp drops by up to 2°C in the plume, explained by the flight path through the top of the plume where the UAV encountered cooling air.

Combining visual evidence, the gradual increase in acceleration up to the two plume points, and the 20% increase in RH, it seems that the plume was descended into on this leg. It was flown through at an altitude of 4,014 m AMSL for approximately 1 min before the aircraft turned at the end of the leg. That the aircraft descended while trying to climb indicated two things: first that the original motor type on the Skywalker was severely limiting in these conditions, and second that the air above the plume drew the aircraft down. Effects, such as the circulation of matter in the plume, could explain this uncommanded movement.

#### 5.4 | Flight D

This mission varies from the others presented here most notably because there was a section of piloted flight, albeit with augmentation from the autopilot. Figure 7 clearly shows that the plume was flown through. Where previous flights intercepted the plume at least 1.8 km from the crater, this one was approximately 0.6 km from the crater. Before the plume contact the UAV overflowed the crater and loitered for 4 min.

Figure 17 shows data from the initial summit overflight until after the piloted section of flight (see Figure 16). Note the magnitude of the acceleration data in Figure 17; the vertical accelerations recorded were up to four times greater than anything previously flown through. This can be attributed to the state of the plume at this distance from the summit, as it is still visually turbulent and not yet at neutral buoyancy (i.e., it is still rising, albeit at a slower rate than after initial expulsion). The pitch data also indicate turbulence at the plume point, however little else can be gleaned from the pitch or throttle data for this flight due to the aircraft mode. Fully automated flight would have enabled a more thorough analysis of the plume from an aircraft control perspective.

The nonneutral buoyancy observed suggested that there would be an increase in temperature during the fly-through. Figure 18 shows a relatively consistent temperature of 3.7°C during loitering flight and an increase of approximately 1.1°C during the plume fly-through. The AMP Temp registered approximately 0.9°C higher than the iMet, but peaked only around 0.5°C in the plume. The differences could be explained by calibration errors, however the sensors agree that in this instance the in-plume temperature is higher than ambient temperature, and is approximately 5°C.

RH data showed similar responses to the temperature, with a consistent 64% during the loiter phase and an increase to 74% in the plume. The iMet has previously shown a 20% RH increase in the plume, but here it is only 10%. One explanation for this is the mounting location of the sensor, as for this flight it was located in the nose rather than on the outside of the fuselage. The iMet data respond with acceptable levels of delay when compared to the flight data turbulence, however further testing of response times at flight speed is needed to confirm the exact point at which RH increases relative to the Z-axis acceleration.

#### 5.5 | In-plume-detection metric

As shown in Figures 12, 15, and 19,  $P_{InPlume}$  generates a value that peaks at the identified plume points of the flights. In addition to the previously identified plume points there are some additional unity values shown, such as in Figure 19 where there are peaks at around 27 min. It is suggested that the metric presented in this paper is a good indicator of UAV/plume interaction, and that it should be used in real-time for operational decision making when targeting plume fly-throughs. Further testing could include the inclusion of CO<sub>2</sub> or SO<sub>2</sub> sensors, which should sense changes in the plume compared to in ambient air. These could be included provided they are capable of sensing the expected change, are suitably light, and have low power requirements.

### 6 | CONCLUSIONS AND FURTHER WORK

This paper has shown that fixed-wing UAVs can be used to collect small ash samples from the plume of Volcán de Fuego in Guatemala. Flight B here proves the concept of airborne ash collection using SEM stubs. Given an appropriate collection mechanism, the aerial sampling of ash with a representative PSD from within a plume has been shown to be possible. These data shall be used to better model the effects of volcanic ash on aircraft and be input into active aviation management tools.

Vertical acceleration of the aircraft was combined with altitude, pressure data, and humidity data to identify when the UAV was in a plume. These data were then combined to form  $P_{InPlume}$ , which reached a value of 1 when the aircraft was in a plume over the three applicable flights presented here. Additional sensors, such as gas sensors, could be added for the generation of  $P_{InPlume}$ , provided they add to the robustness of the metric and are suitably small and lightweight.

The team succeeded in finding a *modus operandi* which results in successful UAV flights for monitoring the volcano. With proper automation and education, the levels of expertise required to carry out monitoring missions can be reduced such that a wider range of people and local agencies could use the technology developed here.

Future aims of this project include flying through the plume using an automated tracking algorithm that considers the wind speed and direction, the input being a real-time implementation of the in-plume-

detection metric developed in this paper. This would enable sampling ash at a proximal point, then as the plume moves downwind sampling again from the same point at predefined radial distances. The analysis of these samples would then give the rate at which ash falls out of the plume, an important characteristic for aviation management. The automation of this process should increase reliability and repeatability.

Additional further work includes the development of a real-time trajectory planner that uses on-board computing to find a suitable, near-optimal, path to the area of interest, taking into account obstacles in the airspace and aircraft flight performance. These flights could be made into long endurance missions by incorporating energy scavenging algorithms. BVLOS operations with multiple airborne UAVs are also of interest, possibly to collect different data types from the same plume. The conditions around the crater will be investigated by deploying single-use remote sensors from the aircraft which will send data back to the operator in real-time.

## ACKNOWLEDGEMENTS

The flights and work that went into this paper would not have been possible without the kind and generous help afforded to the team by INSIVUMEH, the Guatemalan Institute of Seismology, Volcanology, Meteorology, and Hydrology. Thanks also to DGAC, the Guatemalan National Aviation Authority, who approved the flight plans and placed NOTAMS as necessary, and to GeoTravel Guatemala for local knowledge, interpretation, and transport. Thanks also to the developers of ArduPilot and Mission Planner. The funding for this study came in part from the CASCADE (Complex Autonomous aircraft Systems Configuration, Analysis and Design Exploratory) programme grant (EP/R009953/1).

## ORCID

Ben Schellenberg  <http://orcid.org/0000-0002-7296-6512>

Kieran Wood  <http://orcid.org/0000-0002-5804-7704>

## REFERENCES

- Altstädter, B., Platis, A., Wehner, B., Scholtz, A., Wildmann, N., Hermann, M., ... Lampert, A. (2015). ALADINA—An unmanned research aircraft for observing vertical and horizontal distributions of ultrafine particles within the atmospheric boundary layer. *Atmospheric Measurement Techniques*, 8, 1627–1639.
- Amici, S., Turci, M., Giulietti, F., Giammanco, S., Buongiorno, M. F., LaSpina, A., & Spampinato, L. (2013). Volcanic environments monitoring by drones mud volcano case study. *ISPRS—International Archives of the Photogrammetry, Remote Sensing and Spatial Information Sciences*, XL-1/W2(May 2014), 5–10.
- Clarkson, R. J., Majewicz, E. J. E., & Mack, P. (2016). A re-evaluation of the 2010 quantitative understanding of the effects volcanic ash has on gas turbine engines. *Proceedings of the Institution of Mechanical Engineers, Part G: Journal of Aerospace Engineering*, 230(12), 2274–2291.
- Di Stefano, G., Romeo, G., Mazzini, A., Iarocci, A., Hadi, S., & Pelphrey, S. (2017). The Lusi drone: A multidisciplinary tool to access extreme environments. *Marine and Petroleum Geology*, 30(December), 1–12.
- Everaerts, J. (2008). The use of unmanned aerial vehicles (UAVs) for remote sensing and mapping. *The International Archives of the Photogrammetry, Remote Sensing and Spatial Information Sciences*, 37(B1), 1187–1192.
- Google Earth. (2018). <https://earth.google.com/web/>
- Greatwood, C., Richardson, T., Freer, J., Thomas, R., Brownlow, R., Lowry, D., ... Nisbet, E. (2016). Automatic path generation for multirotor descents through varying air masses above Ascension Island. In *Proceedings of the AIAA SciTech Forum*, San Diego, CA, USA, January 2016 (pp. 1–12).
- Greatwood, C., Richardson, T. S., Freer, J., Thomas, R. M., Rob Mackenzie, A., Brownlow, R., ... Nisbet, E. G. (2017). Atmospheric sampling on Ascension Island using multirotor UAVs. *Sensors (Switzerland)*, 17(6), 1–24.
- Jordan, B. R. (2015). A bird's-eye view of geology: The use of micro drones/UAVs in geologic fieldwork and education. *GSA Today*, 25(7), 50–52.
- Klemas, V. V. (2015). Coastal and environmental remote sensing from unmanned aerial vehicles: An overview. *Journal of Coastal Research*, 31(5), 1260–1267.
- Letheren, B., & Montes, G. (2016). Design and flight testing of a bio-inspired plume tracking algorithm for unmanned aerial vehicles. In *2016 IEEE Conference, IEEE, Big Sky, MT, USA* (pp. 1–9).
- Longo, D., Melita, C., Muscato, G., & Giudice, G. (2014). Measurement and exploration in volcanic environments. In Vachtsevanos, G. J., & Valavanis, K. P. (Eds.), *Handbook of unmanned aerial vehicles* (pp. 2667–2692). Dordrecht: Springer.
- McGonigle, A. J. S., Aiuppa, A., Giudice, G., Tamburello, G., Hodson, A. J., & Gurreri, S. (2008). Unmanned aerial vehicle measurements of volcanic carbon dioxide fluxes. *Geophysical Research Letters*, 35(6), 3–6.
- Mishchenko, M. I. (1993). Light scattering by size-shape distributions of randomly oriented axially symmetric particles of a size comparable to a wavelength. *Applied Optics*, 32(24), 4652–4666.
- Montes, G., Letheren, B., Villa, T., & Gonzalez, F. (2014). Bio-inspired plume tracking algorithm for UAVs. In *Australasian Conference on Robotics and Automation, 2-4 December 2014, The University of Melbourne, Victoria, Australia Australasian Conference on Robotics and Automation (ACRA), 02-04- Dece*.
- Ogiso, M., Matsubayashi, H., Yamamoto, T., Murase, M., Kimata, F., Yamanaka, Y., ... Tanaka, R. (2016). Volcanic plume measurements using a UAV for the 2014 Mt. Ontake eruption. *Earth, Planets and Space*, 68(1), 49.
- Paredes, J. A., Saito, C., Abarca, M., & Cuellar, F. (2017). Study of effects of high-altitude environments on multicopter and fixed-wing UAVs' energy consumption and flight time. In *2017 13th IEEE Conference on Automation Science and Engineering (CASE)* (pp. 1645–1650).
- Pieri, D., Diaz, J. A., Bland, G., Fladeland, M., Madrigal, Y., Corrales, E., ... Rica, C. (2013). In situ observations and sampling of volcanic emissions with NASA and UCR unmanned aircraft, including a case study at Turrialba Volcano, Costa Rica, London: Geological Society.
- Prata, A. J., Volcanic, F. O. R., & Clouds, A. S. H. (1989). Infrared radiative transfer calculations for volcanic ash clouds. *Geophysical Research Letters*, 16(11), 1293–1296.
- Ramanathan, V., Ramana, M. V., Roberts, G., Kim, D., Corrigan, C., Chung, C., & Winker, D. (2007). Warming trends in Asia amplified by brown cloud solar absorption. *Nature*, 448(7153), 575–578.
- Schuyler, T. J., & Guzman, M. I. (2017). Unmanned aerial systems for monitoring trace tropospheric gases. *Atmosphere*, 8(206).
- Smithsonian Institute. (2002). <https://volcano.si.edu/volcano.cfm?vn=342090&vtab=GeneralInfo>
- Stix, J., Moor, J. M. D., Rüdiger, J., Alan, A., Corrales, E., Arcy, F. D., ... Liotta, M. (2018). Journal of geophysical research: Solid earth using drones and miniaturized instrumentation to study degassing at Turrialba and Masaya volcanoes, Central America. *Journal of Geophysical Research: Solid Earth*, 2013, 1–20.

- Stohl, A., Prata, A. J., Eckhardt, S., Clarisse, L., Durant, A., Henne, S., ... Weinzierl, B. (2011). Determination of time- and height-resolved volcanic ash emissions and their use for quantitative ash dispersion modeling: The 2010 Eyjafjallajökull eruption. *Atmospheric Chemistry and Physics*, 11(9), 4333–4351.
- Stull, R. B. (2005). *Meteorology for scientists and engineers* (2nd ed., pp. 705–714).
- Thomas, H. E., & Watson, I. M. (2010). Observations of volcanic emissions from space: Current and future perspectives. *Natural Hazards*, 54(2), 323–354.
- Thomas, R. M., Lehmann, K., Nguyen, H., Jackson, D. L., Wolfe, D., & Ramanathan, V. (2012). Measurement of turbulent water vapor fluxes using a lightweight unmanned aerial vehicle system. *Atmospheric Measurement Techniques*, 5(1), 243–257.
- Thomas, R. M., Mackenzie, A. R., Reynolds, S. J., Sadler, J. P., Cropley, F., Bell, S., ... Cai, X. (2018). Avian sensor packages for meteorological measurements. *Bulletin of the American Meteorological Society*, 99(3), 499–511.
- U.S. Department of Interior (2013). *Oblique photogrammetry to monitor volcanoes*. U.S. Department of Interior, USA
- Villa, T. F., Gonzalez, F., Milijevic, B., Ristovski, Z. D., & Morawska, L. (2016). An overview of small unmanned aerial vehicles for air quality measurements: Present applications and future perspectives. *Sensors*, 16, 12–20.
- Watson, I. M., Realmuto, V. J., Rose, W. I., Prata, A. J., Bluth, G. J. S., Gu, Y., ... Yu, T. (2004). Thermal infrared remote sensing of volcanic emissions using the moderate resolution imaging spectroradiometer. *Journal of Volcanology and Geothermal Research*, 135(1-2), 75–89.
- Wegener, S. S. (2004). UAV autonomous operations for airborne science missions. In *AIAA 3rd "Unmanned Unlimited" Technical Conference, Workshop and Exhibit*, September 2004 (pp. 1–10). Chicago, Illinois.
- Western, L. M., Watson, M. I., & Francis, P. N. (2015). Uncertainty in two-channel infrared remote sensing retrievals of a well-characterised volcanic ash cloud. *Bulletin of Volcanology*, 77(8), 67.
- Wilcox, E. M., Thomas, R. M., Praveen, P. S., Pistone, K., Bender, F. A.-M., & Ramanathan, V. (2016). Black carbon solar absorption suppresses turbulence in the atmospheric boundary layer. *Proceedings of the National Academy of Sciences*, 113(42), 11794–11799.

## SUPPORTING INFORMATION

Additional supporting information may be found online in the Supporting Information section.

**How to cite this article:** Schellenberg B, Richardson T, Watson M, et al. Remote sensing & identification of volcanic plumes using fixed-wing UAVs over Volcán de Fuego, Guatemala. *J Field Robotics*. 2019;36:1192–1211. <https://doi.org/10.1002/rob.21896>

## APPENDIX: INDEX TO MULTIMEDIA EXTENSIONS

Four video files have been submitted alongside this paper, one for each of the four flights presented. These files have been compressed into \*.avi versions to meet submission requirements.

Filename	Media type	Description
FlightA.avi	Video	Video of high-altitude and plume section of Flight A
FlightB.avi	Video	Video of high-altitude and plume section of Flight B
FlightC.avi	Video	Video of high-altitude and plume section of Flight C
FlightD.avi	Video	Video of high-altitude and plume section of Flight D